Derivation of aerosol fluorescence and water vapor Raman depolarization ratios from lidar measurements

Igor Veselovskii[1], Qiaoyun Hu[2], Philippe Goloub[2], Thierry Podvin[2], William Boissiere[2], Mikhail Korenskiy[1], Nikita Kasianik[1], Sergey Khaykyn[3], Robin Miri[2]

[1]*Prokhorov General Physics Institute of the Russian Academy of Sciences, Moscow, Russia.*

[2]*Univ. Lille, CNRS, UMR 8518 - LOA - Laboratoire d'Optique Atmosphérique, F-59650 Lille, France*

[3]*Laboratoire Atmosphère Observations Spatiales, UVSQ, CNRS, Sorbonne University, Guyancourt, France*

Correspondence: Qiaoyun Hu (qiaoyun.hu@univ-lille.fr)

Abstract

Polarization properties of the fluorescence induced by polarized laser radiation are widely considered in laboratory studies. In lidar observations, however, only the total scattered power of fluorescence is analyzed. In this paper we present results obtained with a modified Mie-Raman-Fluorescence lidar operated at the ATOLL observatory, Laboratoire d'Optique Atmosphérique, University of Lille, France, allowing to measure depolarization ratios of fluorescence at 466 nm (δ_F) and of water vapor Raman backscatter. Measurements were performed in May-June 2023 during Alberta forest fires season when smoke plumes were almost continuously transported over the Atlantic Ocean towards Europe. During the same period, smoke plumes from the same sources were also detected and analyzed in Moscow, at General Physics Institute (GPI), with a 5-channel fluorescence lidar able to measure fluorescence backscattering at 438, 472, 513, 560 and 614 nm. Results demonstrate that, inside the boundary layer (BL), urban aerosol fluorescence is maximal at 438 nm, then it gradually decreases with wavelength. Results also show that the maximum of the smoke fluorescence spectrum shifted towards longer wavelengths. The smoke layers observed within 4-6 km present a maximum of fluorescence at 513 nm while, in the upper troposphere (UT), the maximum shifts to 560 nm. Regarding fluorescence depolarization, its value typically varies inside the 45-55 % range, however several smoke plume layers detected above 10 km were characterized by a δ_F increasing up to 70%. Inside the BL, the fluorescence depolarization ratio was higher than that of smoke and varied inside the 50-70% range. Moreover, in the BL, δ_F appears

to vary with atmospheric relative humidity (RH) and, in contrast to the elastic scattering, fluorescence depolarization increases with RH.

The depolarization ratio of the water vapor Raman backscattering is shown to be quite low (2±0.5%) in the absence of fluorescence, because the narrowband interference filter in the water vapor channel selects only strongest vibrational lines of the Raman spectrum. As a result, depolarization of the water vapor Raman backscattering is sensitive to the presence of strongly depolarized fluorescence backscattering. The fluorescence contamination into the water vapor Raman channel can be calculated from the water vapor Raman depolarization ratio with the only assumption that δ_F remains constant within the 408-466 nm range.

1. Introduction

Possibility to measure the laser induced fluorescence becomes an important added-value to existing Mie-Raman lidars, because fluorescence measurements provide new independent information about aerosol properties. Nowadays, the spectroscopic lidars based on 32-channel PMTs combined with spectrograph, proved the ability to measure the fluorescence spectrum (Sugimoto et al., 2012; Reichardt, 2014; Reichardt et al., 2018, 2023, Liu et al., 2022). On the other hand, the lidars, with a single fluorescence channel can be widespread due to their simplicity (Rao et al., 2018; Veselovskii et al., 2020). Such single-channel fluorescence measurements combined with depolarization measurements at elastic wavelength, provide new independent information about aerosol type (Veselovskii et al., 2022; Wang et al., 2023). However, in all lidar studies, only total scattered power was analyzed, while polarization properties of the fluorescence were ignored. At the same time, fluorescence depolarization measurements are widely used in laboratory research (Lakowicz, 2006). When polarized laser radiation is used for excitation, the fluorescence emission is also partly polarized and degree of emission polarization (anisotropy) depends on the fluorescence lifetime, on the angle between excitation and emission dipoles, and on the rotational mobility of molecules (Lakowicz, 2006). In fluorescence spectroscopy the anisotropy is introduced as given by Eq.1:

$$r = \frac{P_F^{\parallel} - P_F^{\perp}}{P_F^{\parallel} + 2P_F^{\perp}} \quad (1)$$

Here $P_F^{\parallel}$ and $P_F^{\perp}$ are the powers of co- and cross-polarized fluorescence components. In lidar measurements, however, a commonly used parameter is the depolarization ratio, δ_F, is given as:

$$\delta_F = \frac{P_F^{\perp}}{P_F^{\parallel}}. \quad (2)$$

Therefore, the anisotropy is expressed as a function of the δ_F as follows:

~~Anisotropy and depolarization ratio are two interconvertible parameters~~

$$r = \frac{1-\delta_F}{1+2\delta_F} \quad (3)$$

For randomly oriented fluorophores with collinear absorption and emission dipoles, in the absence of rotational motion, the anisotropy ~~is~~ r=0.4 (Lakowicz, 2006), which corresponds to δ_F=33%. This is the minimal value one can expect in lidar measurements. Existence of ~~the~~ any angle between absorption and emission dipoles, as well as molecule rotation in the process of emission will increase δ_F. Thus, measurement of fluorescence depolarization ratio may bring additional information about atmospheric aerosol as we will show below. ~~; Moreover, depolarization measurements help to analyze the impact of fluorescence on water vapor Raman measurements~~. ->This is also written in line 82.

Water vapor is a key atmospheric component playing essential role in the planet's radiative balance, and Raman lidars today are widely used for such observations (Whiteman, 2003, Chouza et al., 2022 and references therein). However, when the UV laser beam passes through a smoke layer, the broadband fluorescence signal is induced and its spectrum includes the region of water vapor Raman lines. Thus, the signal in the water vapor channel (around 407.5 nm, when 354.7 nm laser radiation is ~~used for stimulation~~ emitted) becomes contaminated by the fluorescence backscatter signal (Immler et al.. 2005; Immler and Schrems, 2005). This contamination can be reduced by decreasing the width of the transmission band in the water vapor channel down to tenths of nm. However, as it was shown recently, fluorescence still remains ~~the~~ an issue, especially inside the smoke layers in ~~high~~ the upper free troposphere (Chouza et al., 2022; Reichardt et al., 2023). Reichardt et al., 2018

Moreover, d Depolarization measurements provide an opportunity to monitor the presence of fluorescence signal in the Raman channels. The Q-branch of water vapor Raman lines (near 407.5 nm) provides a weakly depolarized backscatter, while fluorescence is strongly depolarized. Thus, the presence of fluorescence should increase the depolarization ratio of signal in the water vapor channel. Moreover, if the depolarization ratios of water vapor and fluorescence are known, the contribution of fluorescence to the measured water vapor mixing ratio (WVMR) can be evaluated.

In this article, we report and analyze, for the first time, the depolarization ratio of aerosol fluorescence and ~~depolarization ratio~~ of water vapor Raman backscatter from lidar observations performed at the ATOLL observatory (ATmospheric Observation at liLLe), Laboratoire

d'Optique Atmosphérique, University of Lille, during dense smoke events that occurred in May - June 2023. We start with a description of the experimental setup in Sect.2.1 and derive, in Sect. 2.2, the main equations for estimating the fluorescence contribution to the water vapor Raman channel. In the first part of the results section (Sect.3.1), the fluorescence depolarization ratio over ATOLL is analyzed for different aerosol types. The measurements of fluorescence spectra performed with a new five-channel fluorescence lidar, operated in Moscow, are presented in Sect.3.2. In Sect. 3.3, we analyze depolarization in the water vapor Raman channel and estimate the contamination of fluorescence to the derived WVMR. The article ended with a conclusion.

2. Experimental setup and data analysis

2.1 Lidar system

In our study, two lidar systems were considered. The first one, LILAS ((LIlle Lidar AtmosphereS) is a multiwavelength Mie-Raman-Fluorescence lidar, whereas the second one is a multiwavelength fluorescence lidar operated by General Physics Institute (GPI), Moscow (Veselovskii et al., 2023). Both systems are based on a tripled Nd:YAG laser (Q-Smart 450) with a 20 Hz repetition rate and pulse energy about 100 mJ at 355 nm. Backscattered light in both systems is collected by a 40 cm aperture telescope and the lidar signals are digitized with fiber transient recorders with 7.5 m range resolution, allowing simultaneous detection in the analog and photon counting mode.

LILAS allows the so called $3\beta+2\alpha+3\delta$ configuration, including three particle backscattering (β_{355}, β_{532}, β_{1064}), two extinction (α_{355}, α_{532}) coefficients along with three particle depolarization ratios. The Raman channel with 407.54/0.3 nm interference filter allows also water vapor profiling. At the end 2019, the lidar was modified to enable fluorescence measurements. A part of the fluorescence spectrum is selected by a wideband interference filter of 44 nm width centered at 466 nm (Veselovskii et al. 2020).

In the fluorescence lidar of GPI only 355 nm wavelength is emitted, while fluorescence is measured in five spectral intervals. The central wavelengths and widths of transmission bands are: 438(29), 472(32), 513(29), 560(40) and 614(54) nm (Veselovskii et al., 2023). Thus, the fluorescence spectrum could be sampled. At GPI, the measurements were performed at an angle of 48 deg to the horizon. The strong sunlight background restricts the fluorescence observations of both systems to nighttime hours.

⊛ I would ask the authors to provide, in the Supplement Section a figure showing the transmission spectra of the 5-wavelengths mentioned, so that the reader can see if there are overlaping transmission curves between the various filters. If any they the authors should refer to any induced errors in the detected lidar signals.

Several properties can be derived from fluorescence. The fluorescence backscattering coefficient, $\beta_{F\lambda}$, at wavelength λ_F, is calculated from the ratio of fluorescence and nitrogen Raman backscattering signals, as described in Veselovskii et al. (2020). We remind that $\beta_{F\lambda}$ is related to fluorescence signals integrated over the filter transmission band D_λ. In Moscow measurements are performed at five wavelengths, and to compare $\beta_{F\lambda}$ between different channels one makes use of the "fluorescence spectral backscattering coefficient" $B_\lambda = \frac{\beta_{F\lambda}}{D_\lambda}$ (fluorescence backscattering per spectral interval). LILAS has only one single fluorescence channel, therefore, when presenting data from LILAS, for the sake of simplicity, one uses notation $\beta_{F466}=\beta_F$. The intensive property characterizing aerosol fluorescence is the fluorescence capacity $G_{F\lambda}$, which is the ratio of the fluorescence backscattering at wavelength λ_F to backscattering coefficient at laser wavelength $G_{F\lambda} = \frac{\beta_F}{\beta_\lambda}$. This ratio, in principle, can be calculated for any laser wavelength. For LILAS observations $G_{F\lambda}$ is calculated with respect to β_{532}, because β_{532} is derived with rotational Raman scattering and is considered to be the most reliable. And again, when presenting LILAS data, for simplicity one will use notation $G_{F\lambda}=G_F$. In this work, all profiles of aerosol properties are smoothed with the Savitzky – Golay method, using second order polynomials with 8 points in the window.

Additional information about the atmospheric thermodynamic state was available from radiosonde measurements performed at Herstmonceux (UK) and Beauvechain (Belgium) stations, located 160 km and 80 km away from the ATOLL observatory, respectively. When calculating the relative humidity, one then used the water vapor profiles measured by Raman lidar and temperature profiles provided by the radiosonde.

As discussed in ~~the introduction~~, measurements of fluorescence depolarization ratio and depolarization of water vapor Raman backscatter are expected to bring new information about aerosol properties and fluorescence contamination in the water vapor Raman channel. In 2023, LILAS was upgraded to allow depolarization measurements at both 466 nm and 408 nm. Corresponding optical layout is shown in Fig.1. Dichroic mirrors DM separate 387, 408 and 466 nm components, while polarizing cubes split the components with polarizations oriented parallel (s) and perpendicular (p) to the laser polarization. For both channels the polarizing cube PBS251 from ThorLabs was used. Fluorescence depolarization ratio, δ_F, and water vapor Raman scattering

depolarisation ratio, δw , are both defined and calculated as a ratio of the perpendicular to the parallel respective components. Calibration was performed as described in Freudenthaler et al. (2009). The uncertainty of calibration is estimated to be below 15% for both 466 and 408 nm channels.

2.2 *Expressions for estimating fluorescence impact on water vapor measurements.*

As discussed in the recent work from Chouza et al. (2022) and Reichardt et al. (2023), the broadband aerosol fluorescence is expected to contribute to the signal measured in water vapor Raman channel. Below, one provides the basic equations for estimating this contribution, based on the measurements of the depolarization ratio in the water vapor Raman channel. The backscattered radiative power, at the laser wavelength λ_L, from distance z, can be modeled, after background subtraction, by

$$P_L = O(z)\frac{1}{z^2}C_L \beta T_L^{\,2} \tag{4}$$

Here O(z) is the geometrical overlap factor, which is assumed to be the same for all channels, C_L is the range independent constant, including efficiency of the detection channel. T_L is one-way transmission, describing light losses on the way from the lidar to distance z at wavelength λ_L.

$$T_L = \exp\left\{-\int_0^z [\alpha^a(\lambda_L, z') + \alpha^m(\lambda_L, z')]dz'\right\} \tag{5}$$

Backscattering and extinction coefficients contain aerosol (a) and molecular (m) contributions: $\beta_{\lambda_L} = \beta^a_{\lambda_L} + \beta^m_{\lambda_L}$ and $\alpha_{\lambda_L} = \alpha^a_{\lambda_L} + \alpha^m_{\lambda_L}$.

Radiative power in nitrogen Raman, water vapor Raman, and fluorescence channels can be written in a similar way:

$$P_R = O(z)\frac{1}{z^2}C_R \sigma_R N_R T_L T_R \tag{6}$$

$$P_W = O(z)\frac{1}{z^2}C_W N_W \sigma_W T_W T_L \tag{7}$$

$$P_F = O(z)\frac{1}{z^2}C_F \beta_F T_F T_L \tag{8}$$

Here C_R, C_W, C_F are the corresponding range independent constants. Terms T_R, T_V, and T_F are one-way transmissions at wavelengths λ_R, λ_W, λ_F, corresponding to the centers of transmission bands of

the channels. Terms N_R and N_W are the concentrations in nitrogen and water vapor molecules while σ_R, σ_W are their Raman differential scattering cross sections respectively. The fluorescence backscattering coefficient, β_F, is introduced the same way, as described in Veselovskii et al. (2020).

The power of fluorescence signal that leaks to the water vapor channel is:

$$P_{FW} = O(z)\frac{1}{z^2} C_W \beta_{FW} T_W T_L \tag{9}$$

Here β_{FW} is fluorescence backscattering at wavelength λ_W. The WVMR, n_W, can be obtained from Eq.6 and Eq.7, if the calibration constant $K_W = \frac{C_R}{C_W}\frac{\sigma_R}{\sigma_W}$ is known and is given by Eq. 10:

$$n_W = K_W \frac{P_W}{P_R}\frac{T_R}{T_W} \tag{10}$$

The fluorescence backscattering coefficient, β_F, derived from Eq. 6 and Eq.8, also contains the calibration constant K_F. The procedure of calibration is described in Veselovskii et al. (2020). Finally, β_F is given by Eq. 11.

$$\beta_F = K_F n_R \frac{P_F}{P_R}\frac{T_R}{T_F} \tag{11}$$

Here $n_R = \frac{N_R(z)}{N_R(z=0)}$ is relative change of number density of nitrogen molecules with height.

The fluorescence signal in the water vapor channel can be expressed from P_F using parameter η, which depends on ratio of fluorescence cross sections at wavelengths λ_W and λ_F, on the filters width and on efficiency of both channels,

$$P_{FW} = P_F \eta \frac{T_W}{T_F} \tag{12}$$

The signal measured in the water vapor channel, $\tilde{P}_W$, is the addition of both water vapor backscatter, P_W, and the fluorescence backscatter, P_{FW},

$$\tilde{P}_W = P_W + P_{FW} = P_W + P_F \eta \frac{T_W}{T_F} \tag{13}$$

One should remember, that the fluorescence spectrum, even for the same type of aerosol, can vary with altitude and from observation to observation, which influences η. To minimize this influence it is desirable to keep λ_W and λ_F as close as possible.

If the signals in the water vapor Raman and fluorescence channels are separated into co-polarized (II) and cross-polarized ($\perp$) components, in respect to laser polarization state, their powers in water vapor Raman channel are given respectively by Eq. 14 and Eq. 15:

$$\tilde{P}_W^{II} = P_W^{II} + P_F^{II}\eta\frac{T_W}{T_F} \tag{14}$$

$$\tilde{P}_W^{\perp} = P_W^{\perp} + P_F^{\perp}\eta\frac{T_W}{T_F} = \delta_W P_W^{II} + \delta_F P_F^{II}\eta\frac{T_W}{T_F} \tag{15}$$

Here δ_F and δ_W are the fluorescence and water vapor Raman depolarization ratios, defined in Eq. 16:

$$\delta_F = \frac{P_F^{\perp}}{P_F^{II}} \text{ and } \delta_W = \frac{P_W^{\perp}}{P_W^{II}} \tag{16}$$

Here we assume that depolarization ratio of fluorescence is the same at the wavelengths λ_W and λ_F. This assumption is usually valid, because emission is normally from the lowest singlet state, so the depolarization ratio is spectrally independent (Lakowicz, 2006).

Due to the presence of fluorescence, the depolarization ratio measured in the water vapor Raman channel is given by Eq. 17:

$$\tilde{\delta}_W = \frac{\tilde{P}_W^{\perp}}{\tilde{P}_W^{II}} = \frac{\delta_W P_W^{II} + \delta_F P_F^{II}\eta\frac{T_W}{T_F}}{P_W^{II} + P_F^{II}\eta\frac{T_W}{T_F}} \tag{17}$$

Here δ_W is the depolarization ratio that would be measured in the water vapor Raman channel in the absence of atmospheric fluorescence. From Eq. 9, 10, 14, 15, 17 parameter η can be derived from lidar measurements, such as water vapor mixing ratio, $\tilde{n}_V$, depolarization ratio $\tilde{\delta}_W$ and fluorescence backscattering β_F:

$$\eta = \frac{\tilde{n}_W}{\beta_F}\frac{K_F}{K_W}n_R\frac{(1+\delta_F)(\tilde{\delta}_W - \delta_W)}{(1+\tilde{\delta}_W)(\delta_F - \delta_W)} \tag{18}$$

It should be noted that the choice of calibration constants K_F, K_W does not influence η, because $\tilde{n}_W$ and β_F are calculated with the same calibration constants. Finally, the increase of WVMR Δn_W induced by the fluorescence can be calculated following Eq. 19:

$$\Delta n_W = K_W \frac{P_F \eta \frac{T_W}{T_F}}{P_R} \frac{T_R}{T_W} = \frac{K_W}{K_F} \eta \beta_F \frac{1}{n_R} \quad (19)$$

As soon as parameter η is found from Eq.18, we can estimate error Δn_W from β_F, which in case of LILAS is measured at 466 nm. In such estimation we have to assume that relationship between fluorescence at 466 nm and 408 nm is constant (independent of height). Possibility to perform correction from single – channel fluorescence measurements was discussed by Reichardt et al. (2023), where it was shown, that for 466/408 nm channels, correction actually may depend on height. Corresponding analysis based on our measurements will be presented in Sect.3.2.

We should mention, that when depolarization of water vapor Raman is available, the contribution of fluorescence to WVMR can be obtained without using η. From Eq.18 and Eq.19 it comes:

$$\Delta n_W = \tilde{n}_W \frac{(1+\delta_F)\left(\tilde{\delta}_W - \delta_W\right)}{(1+\tilde{\delta}_W)\left(\delta_F - \delta_W\right)} \quad (20)$$

However, such correction can be performed only at low altitudes, where signal-to-noise ratio in cross-polarized water vapor channel is high enough.

3. Experimental results

In May – June 2023, the Canadian forest fires were at the origin of numerous smoke layers observations in a wide range of altitude, ranging from the PBL to the tropopause. The Boreal wildfire season in 2023 started anomalously early. A wildfire in Alberta, Canada at 53.2° N, 115.7° W has produced an intense Pyrocumulonimbus (PyroCb) cloud on 5 May with the minimum satellite-derived infrared brightness temperature of -66° C, which should correspond to 10-11 km altitude according to the local radiosoundings. In order to describe the long-range transport of the smoke plume produced by this event, we use UV absorbing Aerosol Index (AI) measurements by the Ozone Monitoring and Profiling Suite (OMPS) Nadir Mapper (NM) instrument onboard Suomi NPP satellite mission (Flynn et al., 2014). AI is widely used as a proxy of the amount of absorbing aerosols (e.g smoke, dust, ash) and its dimensionless value is proportional to the altitude of the aerosol layers. The AI values above 15 are usually associated with the smoke plumes at or above the tropopause (Peterson et al., 2018 and references therein), whereas the maximum AI value reported by OMPS-NM instrument for the Alberta event amounted to 19.9.

Fig. 2 displays the spatiotemporal evolution of the smoke plume from the Alberta event represented by the areas of enhanced AI observed between 5 – 21 May. The smoke in the upper troposphere and lower stratosphere (UTLS) is carried by the westerly winds, crossing the Atlantic in about 1 week before reaching Moscow region by 15 May. On that date, the Moscow lidar has detected the smoke layer at 10-11 km (see Sect. 2). The plume was then further advected across Eurasia towards northeastern Siberia. By 22 May the smoke plume completes its first circumnavigation (not shown) and passes over Lille on 23 May and then over Moscow for the second time around 27 May. Thus, we can expect, that the smoke layers observed over Lille and Moscow have the same source.

3.1 Variability of fluorescence depolarization ratio

At the first stage of our research we focused on the variability of the fluorescence depolarization ratio with aerosol types. The main attention was paid to smoke particles, because they provide the strongest impact on the Raman water vapor measurements due to their high fluorescence capacity.

Spatio-temporal distributions of the aerosol elastic and fluorescence backscattering coefficients (β_{532} and β_F), on the night 26-27 June 2023, are shown in Fig.3. Dense smoke layer with β_F as high as 7.0×10^{-4} $Mm^{-1}sr^{-1}$ occurs within the 4.0 -10.0 km height range. The relative humidity increases from 40% at 4 km to RH>90% at 7 km where formation of ice crystals starts. Vertical profiles of aerosol elastic and fluorescence backscattering coefficients (β_{532} and β_F), together with fluorescence capacity, are shown in Fig.3c. Inside the smoke layer, G_F is about 3×10^{-4}, which is a typical value for smoke whereas, above 6 km, it decreases due to ice formation. Ice crystals increase the particle depolarization ratio δ_{532} from 3% at 6 km to 20% at 8 km. Fluorescence signals are strongly depolarized. Inside the BL, δ_F is about 60% whereas above 2 km it drops to approximately 45%. The processes of hygroscopic growth and ice formation do not provide a noticeable impact on δ_F value. During May – June observations, the depolarization ratio of smoke varied mainly inside the 45-55% range.

As discussed in our previous publications (Veselovskii, et al., 2022; Hu et al., 2022), the fluorescence capacity of aged smoke varies inside the $(2.5\text{-}5.5)\times10^{-4}$ range, probably due to the changes in smoke composition and conditions of atmospheric transport. However, during Alberta fires, several smoke plumes with high G_F have been observed. The highest fluorescence capacity

was observed on the night 16-17 June 2023. Vertical profiles of aerosol properties for this episode are shown in Fig.4. Dense smoke layers with fluorescence backscattering exceeding 10.0×10^{-4} $Mm^{-1}sr^{-1}$ occurred within 7.0 -9.0 km height range. In this case, the maximal value of fluorescence capacity reached 10.0×10^{-4}. Fluorescence depolarization ratio is about 50% through the entire smoke layer and the process of ice formation (just like in Fig.3d) does not influence δ_F. Thus, in May - June 2023 strong variations of G_F in the $(2.5\text{-}10.0)\times10^{-4}$ range were accompanied by relatively small variations of δ_F remaining in the 45 - 55% interval.

It is known that in the UTLS smoke particles can reach depolarization ratio, δ_{532} , as high as 15-20% (Burton et al., 2015; Haarig et al., 2018; Hu et al., 2019; Ohneiser et al., 2020). High values of the depolarization ratio are usually attributed to the complex internal structure of smoke particles (Mishchenko et al., 2016). Two smoke events in the UTLS, characterized by enhanced δ_{532}, on 28-29 May and 3-4 June 2023, are illustrated on Fig.5. On 28-29 May, three smoke layers, at ~ 3.5, 6.5 and 11.5 km can be distinguished. High depolarization ratios, reaching 40% at altitudes of 9.8-10.5 km, are due to ice clouds. In the lower smoke plumes ranging between 3.5 and 6.5 km, the particle depolarization did not exceed 8%, whereas above 11 km δ_{532} increases to 15%. High values of δ_{532} observed in the UTLS correlate with increase of G_F and with fluorescence depolarization, δ_F, up to 7.0×10^{-4} and 70%, respectively. Similar behavior was observed on 3-4 June, where depolarization ratio, δ_{532}, above 11.5 km increased up to 15%, simultaneously with an increase of G_F and δ_F up to 9.5×10^{-4} and 70% respectively. Thus, change in particle morphology may affect the depolarization ratio of fluorescence. Another possibility is that, in the UTLS, not only the particle structure can change, but composition as well. At the current stage of analysis, we are not yet able to conclude about the mechanisms explaining the increase of fluorescence depolarization in the UTLS.

We did not observe the effect of atmospheric humidity on smoke fluorescence depolarization. However, inside the BL the observed hygroscopic growth was accompanied by an increase of δ_F. During the 9-16 June 2023 period numerous particle hygroscopic growth cases were observed in the BL. One of such cases, on the night of 12-13 June, is shown in Fig.6. The relative humidity increases inside the BL from 50% to 70% causing an increase of β_{532} near the BL top. Depolarization ratio δ_{532} decreases with height, since the particles in the process of hygroscopic growth become more spherical. The fluorescence depolarization ratio, however, increases inside the boundary layer from 50 to 70%.

All results obtained during 9-16 June, showing dependence of δ_F and δ_{532} on the relative humidity, are summarized in Fig.7. Particle depolarization δ_{532} systematically decreased with RH but, on 16 June, this dependence is not monotonic which could be due to the change of aerosol composition with height. At low RH (below 30%), fluorescence depolarization ratio is about 50%. However, at RH about 90%, δ_F increased up to 70%. One possible explanation of δ_F behavior can be an increase of rotational mobility of the molecules in the process of particle water uptake.

3.2 Fluorescence spectrum sampled with a with 5-channel lidar

The results presented in the previous section were obtained with a single channel fluorescence lidar. However, for analyzing the variability of smoke properties (for example, increase of fluorescence capacity with height) it is important to have information about total fluorescence spectrum. Moreover, to estimate the fluorescence contamination in the Raman water vapor channel, a relationship between fluorescence backscattering at 466 nm and 408 nm is used. Thus we need to know the variability of the fluorescence spectrum in the short wavelength region. In our recent work (Veselovskii et al., 2023) we presented the first results obtained with a 5-channel fluorescence lidar in operation at the GPI. This lidar is able to measure fluorescence backscattering in 5 spectral intervals centered at 438, 472, 513, 560, and 614 nm. In May – June 2023, several smoke plumes originating from Alberta fires were transported over Moscow. Although Lille and Moscow are very distant from each other, smoke plumes observed have the same origin, hence the fluorescence spectra measured over Moscow are quite helpful for the analysis of Lille data.

Fig.8 presents fluorescence spectral backscattering coefficients, B_λ, for 3 smoke events detected in the UTLS above 10, 8 and 10 km for 15, 31 May and 20 June 2023, respectively. On 15 and 31 May smoke layers are also present inside the 4-6 km range. Inside the BL the strongest fluorescence is systematically detected in the 438 nm channel while, at higher altitudes, the maxima shifts to 560 nm. As follows from Fig.8d-f, the ratio B_{560}/B_{438} remains in the range 0.4 - 0.7 inside the BL whereas this ratio increases above 2.0 in the UTLS. Thus, for smoke events the maxima of the fluorescence spectrum shifts with height towards longer wavelengths. The ratio B_{513}/β_{355} also increases with height and, above 10 km, it reaches the values of 1×10^{-5} nm^{-1}. In the UTLS, the maximal fluorescence capacity, G_F, measured by LILAS at 466 nm (with 44 nm bandwidth filter) was about 10×10^{-4}. In the smoke layer, the ratio of backscattering coefficients

β_{355}/β_{532} is about 2, so the maximal ratio B_{466}/β_{355} derived from LILAS measurements is about 1.1×10^{-5} nm^{-1}. Thus, values obtained over Lille and over Moscow are in agreement.

The fluorescence spectra obtained for the above mentioned smoke plumes are shown in Fig.9. The values of B_λ are normalized to B_{438}. Inside the BL, the maximum of fluorescence is measured at 438 nm and it decreases with wavelength. In the smoke layers within 4 - 6 km, the maximum of fluorescence is observed at 513 nm while, in the UTLS, the maximum shifts to 560 nm.

When applying Eq.19 to estimate the contribution of smoke fluorescence into the Raman water vapor channel of LILAS, we assume that the ratio of the fluorescence backscattering at 466 nm to 408 nm is constant. For the lidar in operation at GPI, the shortest available wavelength is 438 nm, therefore, at least, one can estimate the variability of the ratio B_{472}/B_{438}. Fig. 10 presents vertical profiles of B_{472}/B_{438} for 11 smoke events occurring during the 15 May – 20 June 2023 period. Inside the BL, this ratio varies in the 0.6 – 1.0 range. Lowest values correspond to urban aerosols while, values of B_{472}/B_{438} close to 1.0, probably indicate the presence of smoke particles inside the BL. Smoke layers start mainly above 4.0 km and B_{472}/B_{438} shows a tendency to increase in the UT. It is interesting that, for the period 15 May – 1 June, the ratio was close to 1.5 whereas after 1 June, it became close to 1.0, which can be related to changing of smoke source. Mean value of B_{472}/B_{438} in the 4.0 – 11.0 km range over all observations is 1.38 with standard deviation of 0.23 (relative variation is about 17%). The wavelength separation between 466 nm and 408 nm channels is 1.7 larger, so one can expect variation of B_{466}/B_{408} in the smoke layer up to ~30%. This is a very rough estimation, but it points out the difficulties to face when the estimation of the fluorescence contamination to the Raman water vapor channel is performed from a single fluorescence channel at 466 nm. This issue was also discussed in the publication of Reichardt et al. (2023).

3.3 Estimation of fluorescence impact on water vapor Raman measurements

Measuring the depolarization ratio in the water vapor Raman channel provides an opportunity to control/evaluate the presence of fluorescence leak in this channel. These depolarization measurements were performed in Lille during May – June 2023. Vertical profiles of water vapor depolarization ratio $\tilde{\delta}_W$ together with $\tilde{n}_W$, β_{532}, β_F, and G_F are shown in Fig.11 for the night 8-9 and 10-11 June 2023. On 8-9 June aerosols are confined mainly below 5 km. The fluorescence capacity is about 1.0×10^{-4} below 3.0 km, but above, G_F increases up to 2.5×10^{-4},

indicating to the presence of smoke. The depolarization ratio in the water vapor channel is about 2% in the height range 1.5 km – 3.5 km. The values of $\tilde{\delta}_W$ ranging inside 1.8%÷2.0% were observed for this height range, where contribution of fluorescence was insignificant. Depolarization ratio δ_W is low, because the interference filter in water vapor channel selects only strongest Q-branch lines and most of rotational lines are blocked. Contribution of fluorescence becomes noticeable above 3.5 km where n_W drops, resulting in an increase of $\tilde{\delta}_W$ up to ~3%. There is also increase of $\tilde{\delta}_W$ up to 2.2% below 1.0 km, where fluorescence backscattering is enhanced. Similar values of $\tilde{\delta}_W$ were observed on 10-11 June, where depolarization ratio increases up to 2.5% inside the smoke layer observed at ~3.75 km and below 2.0 km.

As discussed in section 2.2, the contribution of fluorescence to the WVMR can be derived from Eq.20 if $\tilde{\delta}_W$ and δ_F are measured. Fig.12 presents the modeling of the relative error $\frac{\Delta n_W}{\tilde{n}_W}$, introduced by the fluorescence to WVMR as a function of $\tilde{\delta}_W$. Computations are performed for fluorescence depolarization ratio δ_F=50%, 60%, 70% to include both smoke and urban particles. Depolarization ratio in the Raman water vapor channel in the absence of fluorescence was assumed to be δ_W=2%. For depolarization ratio $\tilde{\delta}_W$ below 3% the relative error $\frac{\Delta n_W}{\tilde{n}_W}$ did not exceed 3%.

As follows from the fluorescence spectra in Fig.9, the fluorescence of urban particles increases towards short wavelengths, thus one can expect impact of the urban aerosol fluorescence on vapor measurements. In practices, however, we did not observe $\tilde{\delta}_W$ exceeding 3% in the BL, thus, contribution of aerosol in the BL is not critical. The reason is due to the low fluorescence capacity (about one order lower than that of smoke) and higher water vapor content, comparing to free troposphere.

Profiles of $\tilde{\delta}_W$ shown in Fig.11 become noisy at heights where n_W is low, and $\tilde{\delta}_W$ can not be used for correction of fluorescence effect in the UT. To overcome this, one derived the parameter η from Eq.18 at low altitudes where $\tilde{\delta}_W$ is available, and, then, this η is used to calculate Δn_W from Eq.19 in the entire height range. In such an approach, however, one has to assume that relationship between fluorescence cross sections at 466 nm and 408 nm remains constant with height. As

discussed in previous section, such assumption can yield significant bias in calculation of Δn_W, and, at this stage, we do not provide corrected profiles of WVMR.

For accurate calculation of η one needs smoke events with strongly enhanced $\tilde{\delta}_W$, which is usually observed in the dry smoke layers. Such suitable events are shown for the night 26-27 May and 5-6 June 2023 in Fig.13. On 26-27 May a smoke layer characterized by high fluorescence (β_F up to 5×10^{-4} $Mm^{-1}sr^{-1}$) and low $\tilde{n}_W$ (below 0.2 g/kg) is observed at 3.5 km. Fluorescence depolarization ratio is about 47% and $\tilde{\delta}_W$ increases from 2% up to 12% in the middle of this layer. Parameter η calculated from Eq.18 inside this smoke layer is about 2×10^{-3} (g/kg)/($Mm^{-1}sr^{-1}$). On 5-6 June the depolarization ratio $\tilde{\delta}_W$ in the smoke layer increased up to 10% and value of η is very similar. Parameters η derived for several smoke episodes vary in the range $(2\div2.5)\times10^{-3}$ (g/kg)/($Mm^{-1}sr^{-1}$). For the estimate of Δn_W one used the mean value of $\eta=2.25\times10^{-3}$ (g/kg)/($Mm^{-1}sr^{-1}$), which is suitable only for smoke, while for particles in the BL, η can be different. However, in the BL, low depolarization ratios $\tilde{\delta}_W$ prevented us from calculating η.

Fig.14 presents vertical profiles of WVMR, fluorescence backscattering and error Δn_W introduced by the fluorescence in WVMR on 26-27 May, 28-29 May and 16-17 June. Smoke layers with strong fluorescence occurred systematically in our UT observations. The current LILAS system is not powerful enough for deriving accurate water vapor measurements above 10 km, however increase of $\tilde{n}_W$ in fluorescent smoke layers is visible. We remind that Eq.19 for Δn_W contains factor $\frac{1}{n_R}$ (inverse relative change of nitrogen number density), thus, the fluorescence impact on WVMR increases with height. The uncertainties $\frac{\Delta n_W}{\tilde{n}_W}$ for all events considered are shown in Fig.14d. On 26-27 and 28-29 May the uncertainty at 11 km is of the order of 100%. On 16 June the smoke layer is lower (at 9 km) and the uncertainty is about 50%. Our demonstration shows that smoke fluorescence can significantly impact water vapor measurements. The proposed approach, based on the analysis of the depolarization ratio of the water vapor signal, has potential for estimation of corresponding errors and their correction.

4. Conclusion

Modern fluorescence spectroscopy widely uses depolarization measurements of the fluorescence emission induced by polarized laser radiation. However, in application to lidar atmospheric observations, measurement of fluorescence depolarization ratio, presented in this study, is one of the first efforts in this direction. Analysis of more than 30 spring and summer smoke events allows evaluation of the main aerosol intensive properties, including fluorescence capacity, particle and fluorescence depolarization ratio. The fluorescence capacity varied within $(2.5 \div 10.0)\times10^{-4}$ range while the particle depolarization ratio δ_{532} remained below 10%. However, in spite of strong G_F variation, δ_F was remaining within a relatively narrow interval 45-55%. Additional observations revealed that for smoke plumes in the upper troposphere δ_{532} increased up to 15% and fluorescence depolarization increased up to 70%. At the moment, one cannot fully explain the mechanism responsible for this δ_F increase. It can be related to complex particle internal structure at high altitudes, as well as to the change of the chemical composition, revealed by the shift of the maximum of fluorescence spectra to longer wavelengths in the upper troposphere (Fig. 9).

Inside the BL, the fluorescence depolarization ratio was higher than that of smoke and varied inside the 50-70% range. Moreover, fluorescence depolarization ratio of urban particles strongly depends on the relative humidity and, in contrast to elastic scattering, depolarization of fluorescence increases with RH. One possible origin of this phenomena could be attributed to an increase of rotational mobility of the molecules involved in the process of water uptake since δ_F increases when rotation time of molecules becomes comparable with time of fluorescence emission.

The depolarization ratio of Raman water vapor backscatter, in the absence of fluorescence, appears to be quite low (δ_W=2±0.5%), because the narrowband interference filter in the water vapor channel selects only strong Q-lines of the Raman spectrum. As a result, the depolarization ratio of Raman water vapor backscatter is sensitive to the presence of strongly depolarized fluorescence signals. Contribution of fluorescence to the WVMR can be calculated from $\tilde{\delta}_W$ with the only assumption that δ_F remains constant within 408 - 466 nm. However, the depolarization ratio of Raman water vapor backscatter is weak and measurements are only possible up to the middle troposphere with the lidar used in the work, while the problem of fluorescence interference is the most crucial in UTLS. To solve this problem, one can derive η, a parameter linking fluorescence

at 466 nm and at 408 nm. This parameter is calculated for specific smoke events, at low altitudes, and then is used for processing all observations and altitudes.

Such an approach relies on the assumption that the ratio of fluorescence between 466 nm and 408 nm remains constant and allows only a rough estimation of the correction term for the water vapor mixing ratio, Δn_W. One possible solution to improve accuracy of Δn_W is to implement an additional and shorter wavelength channel (438 nm or even shorter). Another technical solution could be considered as the depolarization ratio of Raman water vapor backscatter is low, therefore the 408 nm component can be efficiently selected with a polarizing cube. The depolarized channel then can be used for fluorescence measurements. Polarizing cube works in a wide spectral range, so one can select the region outside of the water vapor spectrum (400 nm – 418 nm) for fluorescence monitoring. We plan this experiment as well as other innovative approaches with our future high-power fluorescence lidar, LIFE (Laser Induced Fluorescence Explorer), whose start of operation is scheduled at the beginning of 2024.

Data availability. Lidar measurements are available upon request (philippe.goloub@univ-lille.fr).

Author contributions. IV processed the data and wrote the paper. QH and TP performed the measurements in Lille. PG supervised the project and helped with paper preparation. WB modified LILAS for polarization measurements. MK and NK performed the measurements in Moscow. SK analyzed transport of smoke layers and RM derived RH profiles from lidar measurements.

Competing interests. The authors declare that they have no conflict of interests.

Acknowledgement

We acknowledge funding from the CaPPA project funded by the ANR through the PIA under contract ANR-11-LABX-0005-01, the "Hauts de France" Regional Council (project ECRIN) and the European Regional Development Fund (FEDER). ESA/QA4EO program is greatly acknowledged for supporting the observation activity at LOA. The work from Q. Hu was supported by Agence *Nationale* de Recherhce ANR (*ANR-21-ESRE-0013) through the* OBS4CLIM project. Development of fluorescence lidar in Moscow was supported by Russian Science Foundation (project 21-17-00114). The work of S. Khaykin was partly supported by the Agence Nationale de la Recherche (ANR) 21-CE01- 335 0007-01 PyroStrat project.

489

490 **References**

491 Baars, H., et al., Atmos. Chem. Phys., 19, 15183-15198, 2019.

492 Burton, S.P., Hair, J.W., Kahnert, M., Ferrare, R.A., Hostetler, C.A., Cook, A.L., Harper, D.B.,
493 Berkoff, T.A., Seaman, S.T., Collins, J.E., Fenn, M.A., and Rogers, R.R.: Observations of the
494 spectral dependence of linear particle depolarization ratio of aerosols using NASA Langley
495 airborne High Spectral Resolution Lidar, Atmos. Chem. Phys., 15, 13453–13473,
496 https://doi.org/10.5194/acp-15-13453-2015, 2015.

497 Chouza, F., Leblanc, T., Brewer, M., Wang, P., Martucci, G., Haefele, A., Vérèmes, H., Duflot,
498 V., Payen, G., and Keckhut, P.: The impact of aerosol fluorescence on long-term water vapor
499 monitoring by Raman lidar and evaluation of a potential correction method, Atmos. Meas.
500 Tech., 15, 4241–4256, https://doi.org/10.5194/amt-15-4241-2022, 2022.

501 Flynn, L., Long, C., Wu, X., Evans, R., Beck, C. T., Petropavlovskikh, I., McConville, G.,
502 Yu, W., Zhang, Z., Niu, J., Beach, E., Hao, Y., Pan, C., Sen, B., Novicki, M., Zhou, S., Seftor,
503 C.: Performance of the Ozone Mapping and Profiler Suite (OMPS) products, J. Geophys. Res.
504 Atmos., 119, 6181–6195, 2014. doi:10.1002/2013JD020467

505 Freudenthaler,V., Esselborn, M.,Wiegner, M.,Heese, B., Tesche, M. and co-authors:
506 Depolarization ratio profiling at severalwavelengths in pure Saharan dust during SAMUM
507 2006, *Tellus* 61B, 165–179, 2009.

508 Haarig, M., Ansmann, A., Baars, H., Jimenez, C., Veselovskii, I., Engelmann, R., and Althausen,
509 D.: Depolarization and lidar ratios at 355, 532, and 1064 nm and microphysical properties of
510 aged tropospheric and stratospheric Canadian wildfire smoke, Atmos. Chem. Phys., 18, 11847-
511 11861, https://doi.org/10.5194/acp-18-11847-2018, 2018.

512 Hu, Q., Goloub, P., Veselovskii, I., Bravo-Aranda, J.-A., Popovici, I. E., Podvin, T., Haeffelin,
513 M., Lopatin, A., Dubovik, O., Pietras, C., Huang, X., Torres, B., and Chen, C.: Long-range-
514 transported Canadian smoke plumes in the lower stratosphere over northern France, Atmos.
515 Chem. Phys., 19, 1173-1193, 2019. https://doi.org/10.5194/acp-19-1173-2019.

516 Hu, Q., Goloub, P., Veselovskii, I., and Podvin, T.: The characterization of long-range transported
517 North American biomass burning plumes: what can a multi-wavelength Mie-Raman-
518 polarization-fluorescence lidar provide? Atmos. Chem. Phys. 22, 5399–5414, 2022
519 https://doi.org/10.5194/acp-22-5399-2022

520 Immler, F. and Schrems, O.: Is fluorescence of biogenic aerosols an issue for Raman lidar
521 measurements? Proc. SPIE 5984, Lidar Technologies, Techniques, and Measurements for
522 Atmospheric Remote Sensing, 59840H, https://doi.org/10.1117/12.628959, 2005.
523 Immler, F., Engelbart, D., and Schrems, O.: Fluorescence from atmospheric aerosol detected by a
524 lidar indicates biogenic particles in the lowermost stratosphere, Atmos. Chem. Phys., 5, 345–
525 355, https://doi.org/10.5194/acp-5-345-2005, 2005.
526 Lakowicz, J. R.: Principles of Fluorescence Spectroscopy, Springer New York, NY, 2006.
527 https://doi.org/10.1007/978-0-387-46312-4
528 Liu, F., Yi, F., He, Y., Yin, Z., Zhang, Y., and Yu, C.: Spectrally Resolved Raman Lidar to
529 Measure Backscatter Spectra of Atmospheric Three-Phase Water and Fluorescent Aerosols
530 Simultaneously: Instrument, Methodology, and Preliminary Results, IEEE Transactions on
531 Geoscience and Remote Sensing, 60, 5703013, 2022, doi: 10.1109/TGRS.2022.3166191
532 Mishchenko MI, Dlugach JM, Liu L. Linear depolarization of lidar returns by aged smoke
533 particles. Appl Opt. 55, 9968-9973, doi: 10.1364/AO.55.009968, 2016.
534 Ohneiser, K., Ansmann, A., Baars, H., Seifert, P., Barja, B., Jimenez, C., Radenz, M., Teisseire,
535 A., Floutsi, A., Haarig, M., Foth, A., Chudnovsky, A., Engelmann, R., Zamorano, F., Bühl,
536 J., and Wandinger, U.: Smoke of extreme Australian bushfires observed in the stratosphere
537 over Punta Arenas, Chile, in January 2020: optical thickness, lidar ratios, and depolarization
538 ratios at 355 and 532 nm, Atmos. Chem. Phys., 20, 8003–8015, https://doi.org/10.5194/acp-
539 20-8003-2020, 2020.
540 Peterson, D.A., Campbell, J.R., Hyer, E.J. et al. Wildfire-driven thunderstorms cause a volcano-
541 like stratospheric injection of smoke, npj Clim. Atmos. Sci. 1, 30, 2018.
542 https://doi.org/10.1038/s41612-018-0039-3
543 Rao, Z., He, T., Hua D, Wang, Y., Wang, X., Chen, Y., Le J.: Preliminary measurements of
544 fluorescent aerosol number concentrations using a laser-induced fluorescence lidar, Appl. Opt.
545 57, 7211-7215, https://doi.org/10.1364/AO.57.007211, 2018.
546 Reichardt, J.: Cloud and aerosol spectroscopy with Raman lidar, J. Atmos. Ocean. Tech., 31,
547 1946–1963, https://doi.org/10.1175/JTECH-D-13-00188.1, 2014.
548 Reichardt, J., Leinweber, R., Schwebe, A.: Fluorescing aerosols and clouds: investigations of co-
549 existence, EPJ Web Conf., 176, 05010, https://doi.org/10.1051/epjconf/201817605010, 2018.

→ Richardson, S., et al., Science of the Total Environment, 696 (2019), 133906

Reichardt, J., Behrendt, O., and Lauermann, F.: Spectrometric fluorescence and Raman lidar: absolute calibration of aerosol fluorescence spectra and fluorescence correction of humidity measurements, Atmos. Meas. Tech., 16, 1–13, 2023. https://doi.org/10.5194/amt-16-1-2023.

Sugimoto, N., Huang, Z., Nishizawa, T., Matsui, I., Tatarov, B.: Fluorescence from atmospheric aerosols observed with a multichannel lidar spectrometer," Opt. Expr. 20, 20800-20807, https://doi.org/10.1364/OE.20.020800, 2012.

Veselovskii, I., Hu, Q., Goloub, P., Podvin, T., Korenskiy, M., Pujol, O., Dubovik, O., Lopatin, A.: Combined use of Mie-Raman and fluorescence lidar observations for improving aerosol characterization: feasibility experiment, Atm. Meas. Tech., 13, 6691–6701, 2020. doi.org/10.5194/amt-13-6691-2020.

Veselovskii, I., Hu, Q., Goloub, P., Podvin, T., Barchunov, B., and Korenskii, M.: Combining Mie–Raman and fluorescence observations: a step forward in aerosol classification with lidar technology, Atmos. Meas. Tech., 15, 4881–4900, 2022b. https://doi.org/10.5194/amt-15-4881-2022.

Veselovskii, I., Kasianik, N., Korenskii, M., Hu, Q., Goloub, P., Podvin, T., and Liu, D.: Multiwavelength fluorescence lidar observations of smoke plumes, Atmos. Meas. Tech., 16, 2055–2065, 2023. https://doi.org/10.5194/amt-16-2055-2023

Wang, Y., Huang, Z., Zhou, T., Bi, J., Shi J.: Identification of fluorescent aerosol observed by a spectroscopic lidar over northwest China, Optics Express, 31, 22157, https://doi.org/10.1364/OE.493557, 2023.

Whiteman, D. N.: Examination of the traditional Raman lidar technique. I. Evaluating the temperature dependent lidar equations, Appl. Optics, 42, 2571–2592, https://doi.org/10.1364/AO.42.002571, 2003.

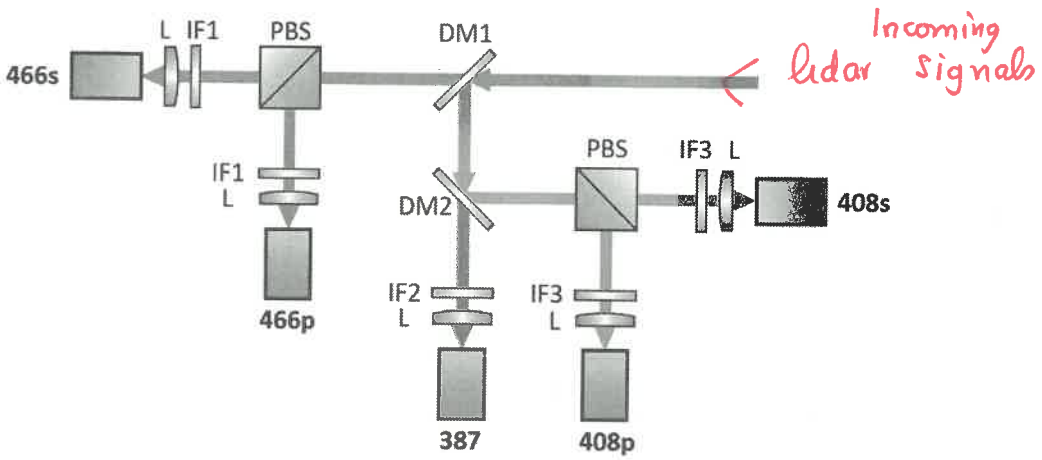

574

575 Fig.1. Optical layout of depolarization measurements at 408 nm and 466 nm wavelengths. L –
576 lens; IF1 - IF3 – interference filters, DM1, DM2 – dichroic mirrors, PBS – polarizing cube.

577

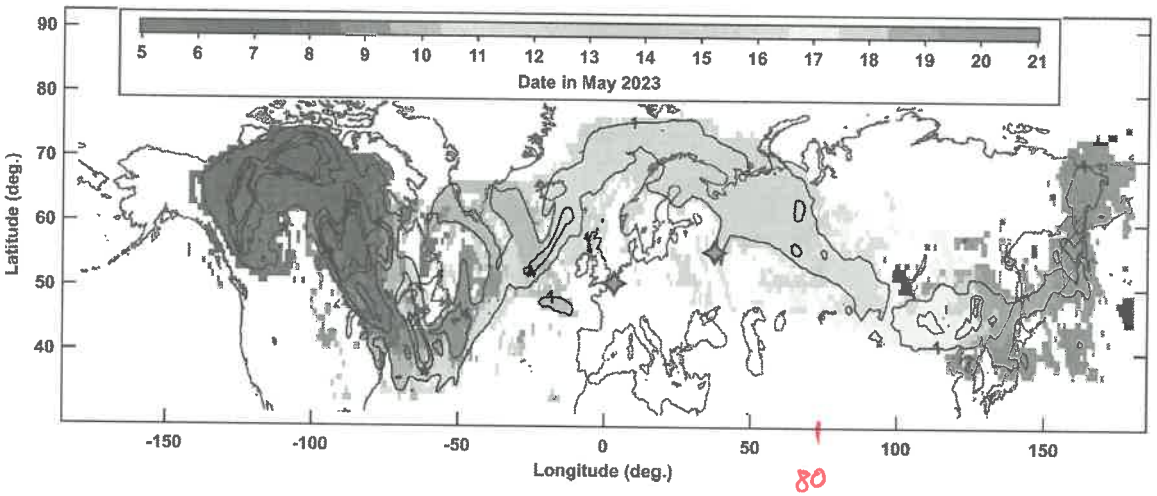

578

579 Fig.2. Spatiotemporal evolution of the smoke plume from the wildfire event in Alberta, Canada on
580 5 May 2023. Color-filled time-coded areas indicate the ~~occurrences of~~ Aerosol Index (AI) values
581 from the OMPS-NPP instrument exceeding 0.5. The actual AI values (1-10) are shown in contours.
582 The blue and red-filled ~~stars~~ stars indicate the location of Lille and Moscow lidar stations respectively.
583

For clarity reasons
* limit the longitude up to 80° !

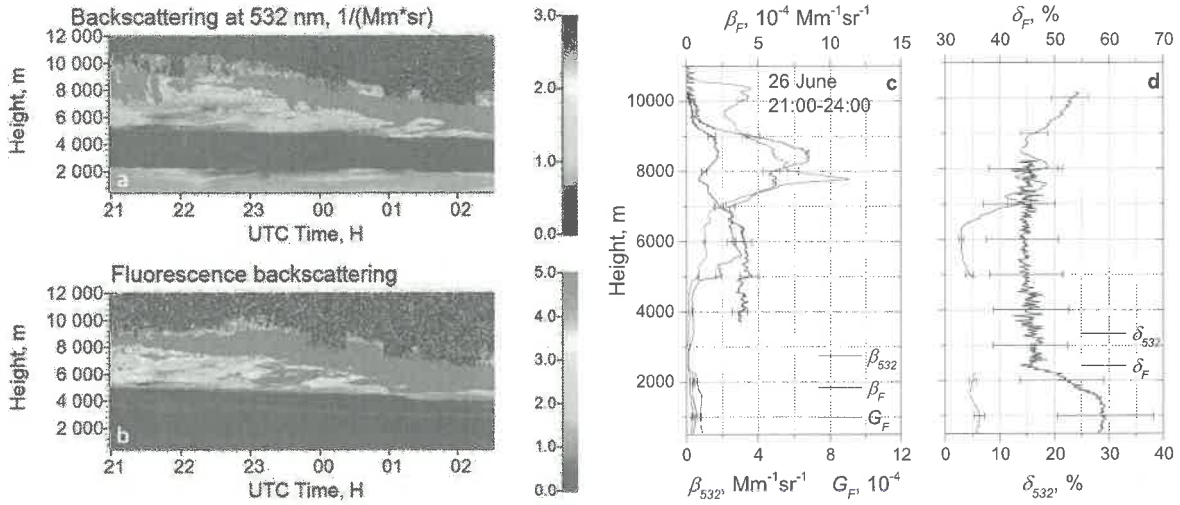

Fig.3. Smoke event on the night 26-27 June 2023. Spatio-temporal distributions of (a) aerosol backscattering coefficient β_{532} and (b) fluorescence backscattering β_F (in 10^{-4} Mm^{-1}sr^{-1}). Vertical profiles of (c) the aerosol β_{532} and fluorescence β_F backscattering coefficients, the fluorescence capacity G_F; (d) the particle δ_{532} and the fluorescence δ_F depolarization ratios.

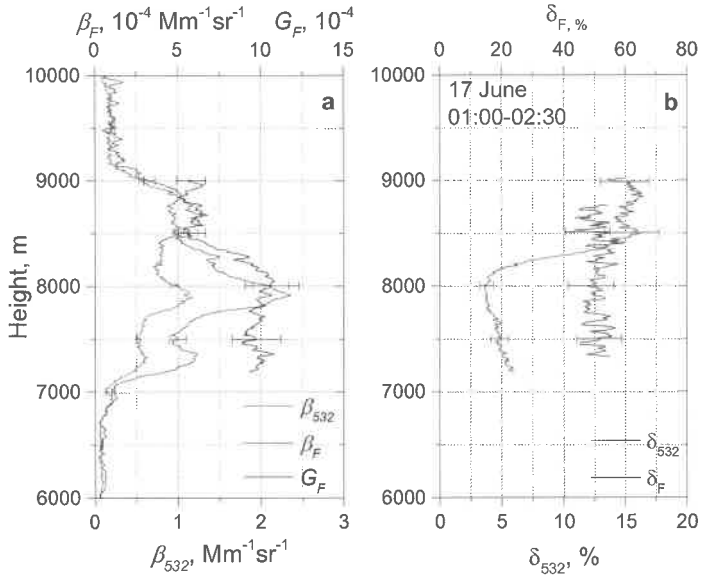

Fig.4. Vertical profiles of (a) aerosol β_{532} and fluorescence β_F backscattering coefficients, fluorescence capacity G_F and (b) particle δ_{532} and fluorescence δ_F depolarization ratios on the night 16-17 June 2023 for period 01:00-02:30 UTC. over.... (define city/region)

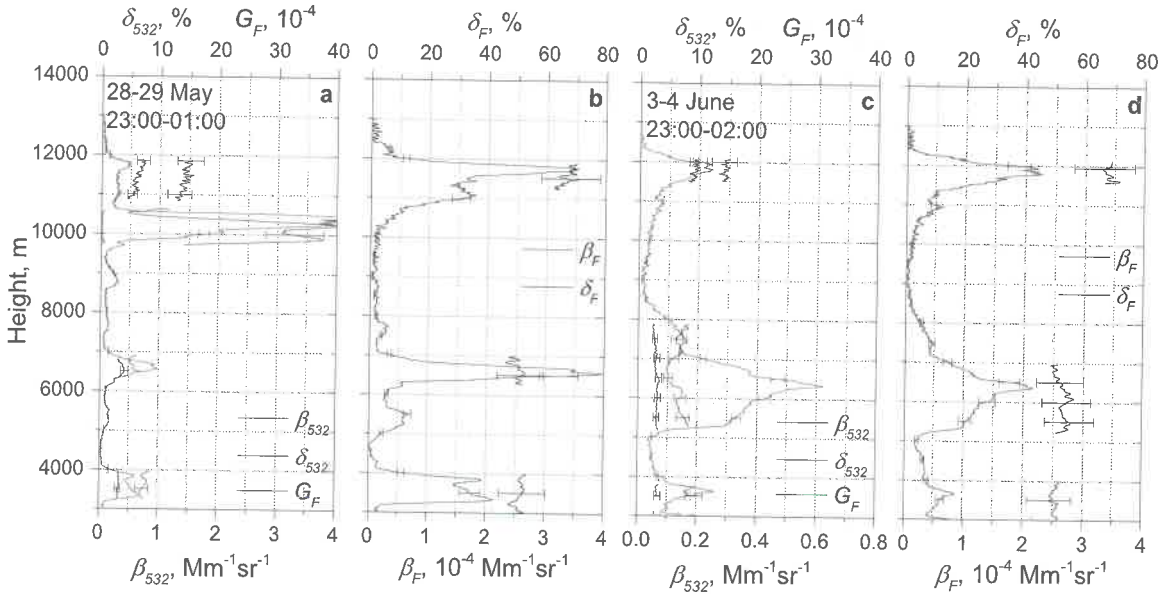

Fig.5. Vertical profiles of (a, c) backscattering coefficient β_{532}, particle depolarization ratio δ_{532}, fluorescence capacity G_F and (b, d) fluorescence backscattering β_F and fluorescence depolarization ratio δ_F for two smoke episodes on the nights 28-29 May 2023 and 3-4 June 2023, over. ... .. define city/region

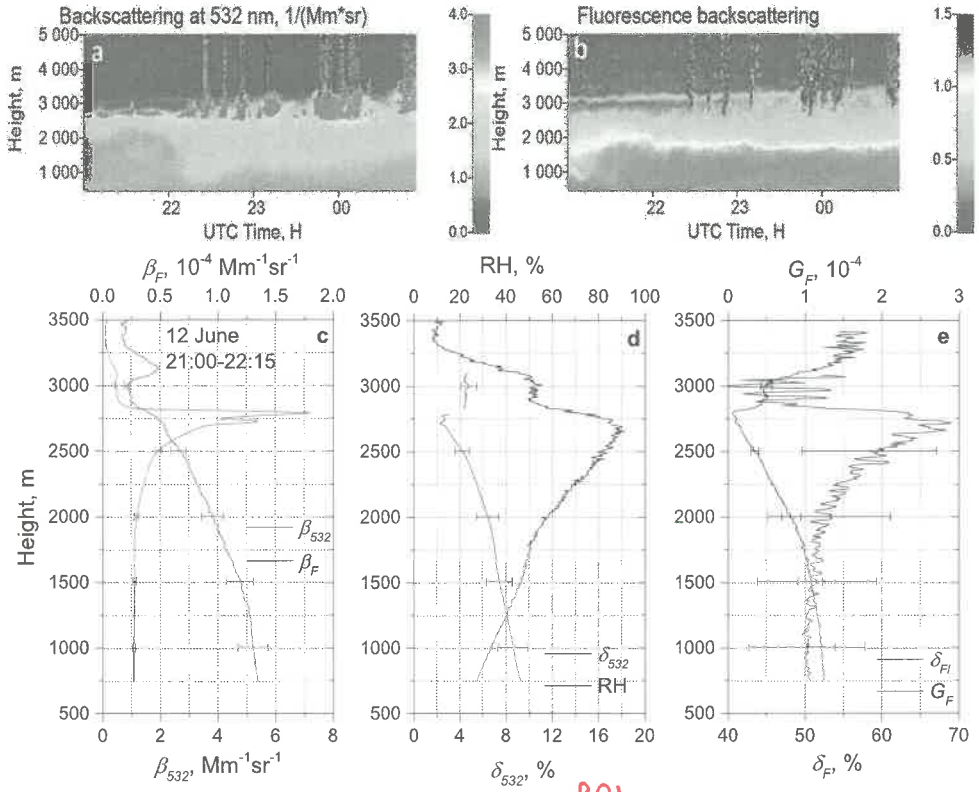

Fig.6. Particle hygroscopic growth in the ~~boundary layer~~ PBL on the night 12-13 June 2023. Spatio-temporal distributions of (a) aerosol backscattering coefficient β_{532} and (b) fluorescence backscattering β_F (in 10^{-4} $Mm^{-1}sr^{-1}$). Vertical profiles of (c) aerosol β_{532} and fluorescence β_F backscattering coefficients; (d) particle depolarization ratio δ_{532} and the relative humidity RH; (e) fluorescence depolarization ratio δ_F and fluorescence capacity G_F for the time period 21:00-22:15 UTC, over..... define region/city

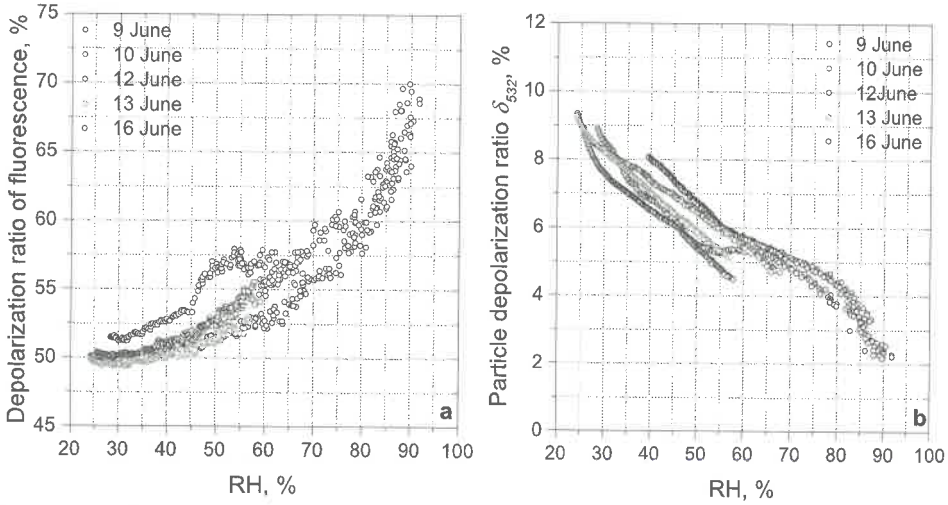

Fig.7. (a) Fluorescence depolarization ratio and (b) particle depolarization ratio δ_{532} as a function of the relative humidity in the ~~boundary layer~~ PBL for the measurements on 9, 10, 12, 13, 16 June 2023, over ..... define city/region

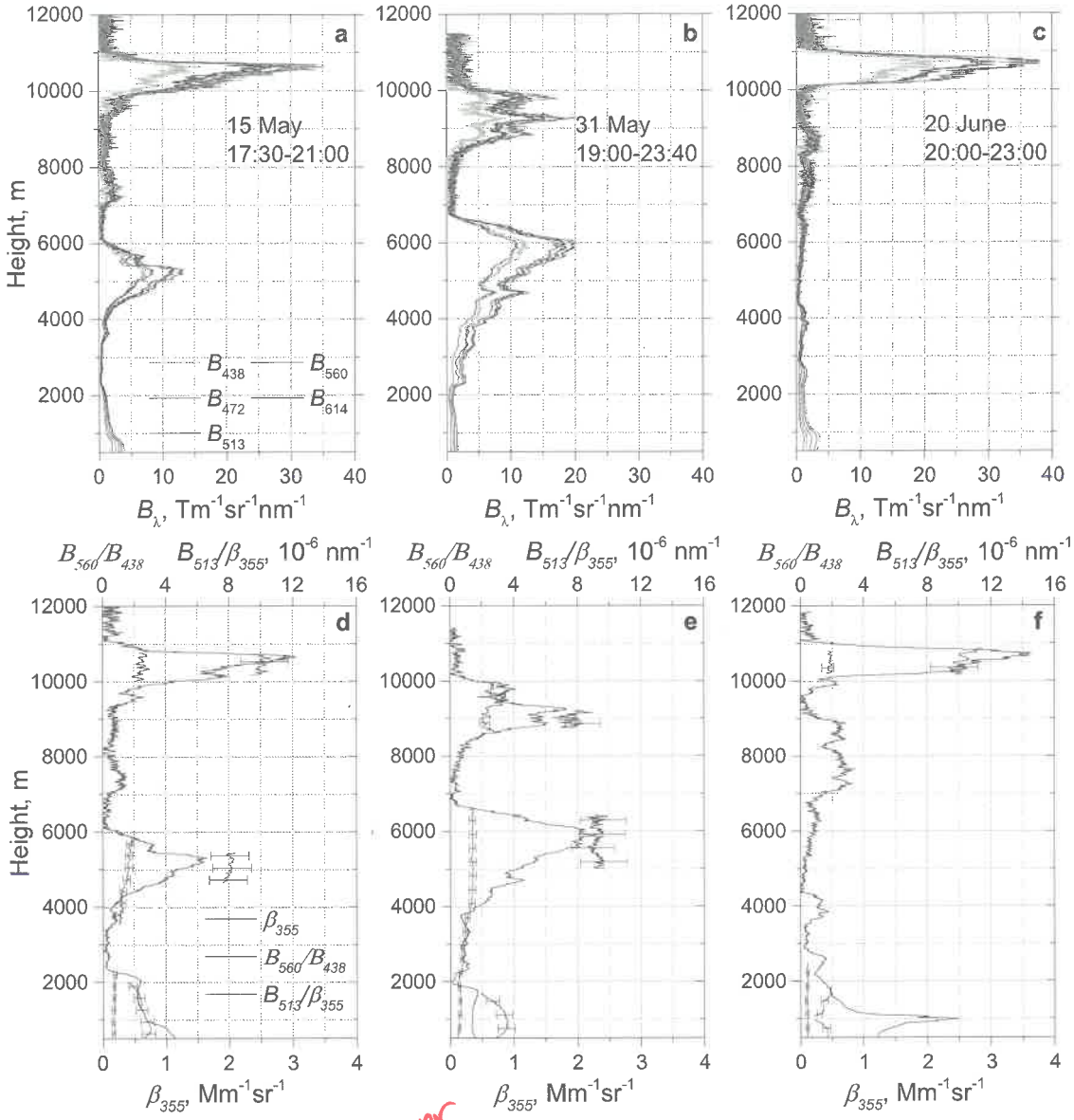

625

626

627 Fig. 8. Fluorescence measurements in Moscow on 15 May, 31 May, 20 June 2023. Vertical profiles
628 of (a-c) fluorescence spectral backscattering coefficients B_λ at 438, 472, 513, 560, 614 nm and (d-
629 f) aerosol backscattering coefficient β_{355}, the ratio B_{560}/B_{438} and B_{513}/β_{355}. Measurements were
630 performed at an angle of 48 deg to horizon.
631

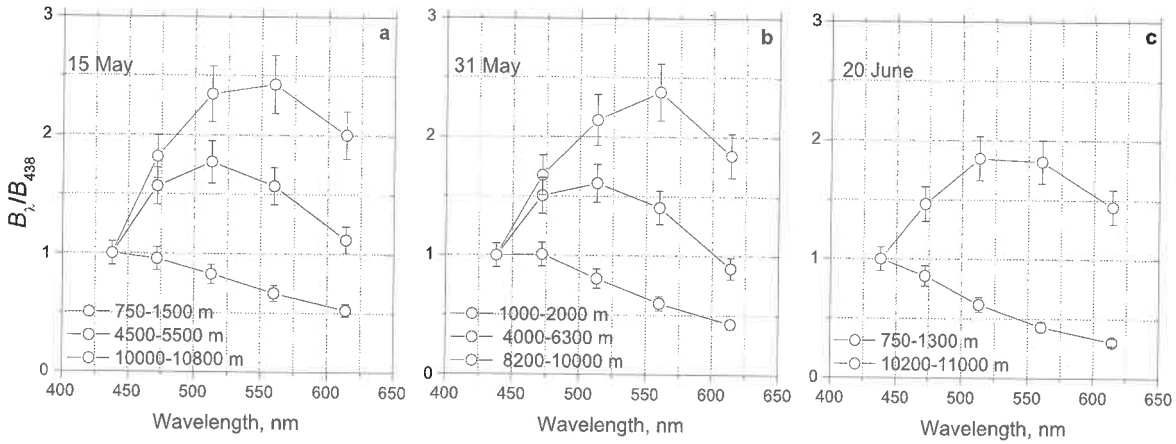

Fig.9. Fluorescence spectra B_λ/B_{438} at different height intervals measured during smoke episodes on 15 May, 31 May, 20 June 2023 for the same temporal intervals as in Fig.8, over Moscow.

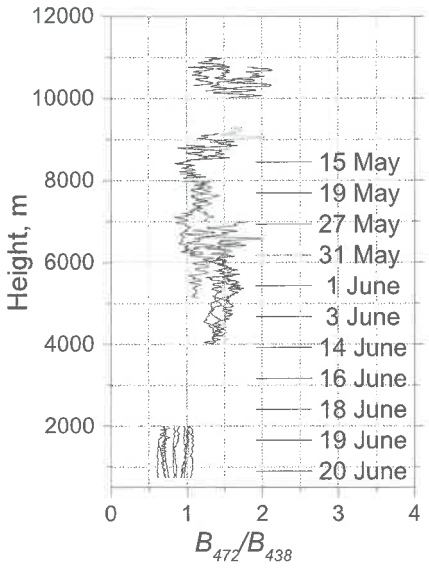

636

637 Fig.10. Height profiles of ratio B_{472}/B_{438} for smoke episodes during 15 May – 20 June 2023. Smoke
638 layers start above ~~4000 m~~.

639

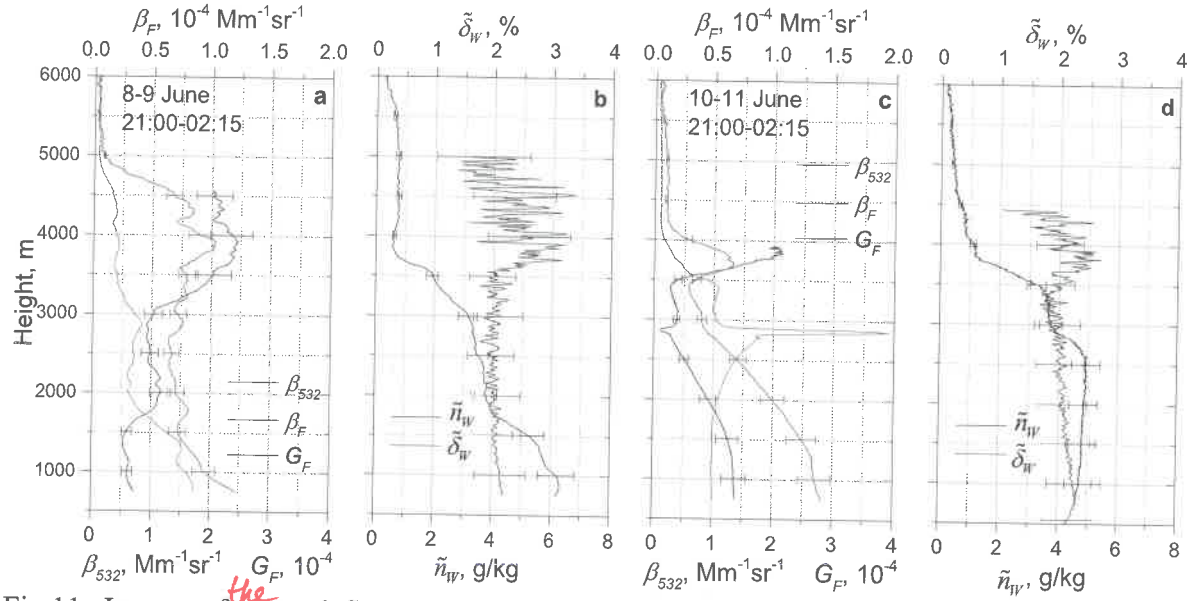

Fig.11. Impact of aerosol fluorescence on the depolarization ratio in the water vapor Raman channel on the nights 8-9 and 10-11 June 2023 at Lille. Vertical profiles of (a, c) particle backscattering β_{532}, fluorescence backscattering β_F, fluorescence capacity G_F and (b, d) depolarization ratio $\tilde{\delta}_W$ of water vapor Raman signal and the water vapor mixing ratio $\tilde{n}_W$.

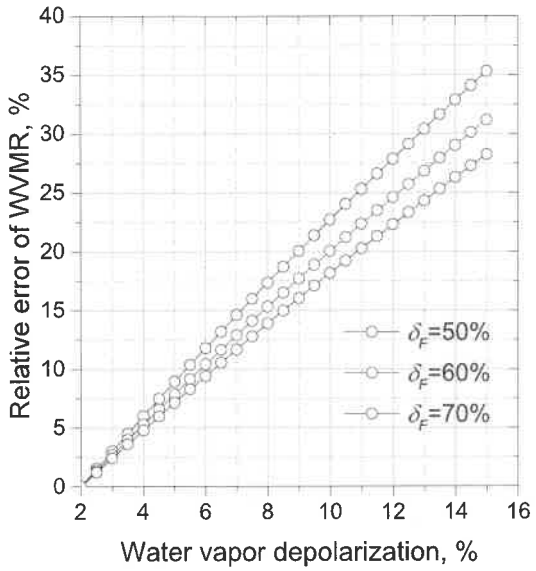

646

647 Fig.12. Relative error of water vapor mixing ratio (WVMR) $\frac{\Delta n_W}{\tilde{n}_W}$ induced by the fluorescence as

648 a function of depolarization ratio $\tilde{\delta}_W$ in the water vapor Raman channel for three values of

649 fluorescence depolarization ratio δ_F=50%, 60%, 70%. The depolarization ratio of water vapor

650 Raman backscatter in the absence of fluorescence is assumed to be δ_W=2%.

651

652

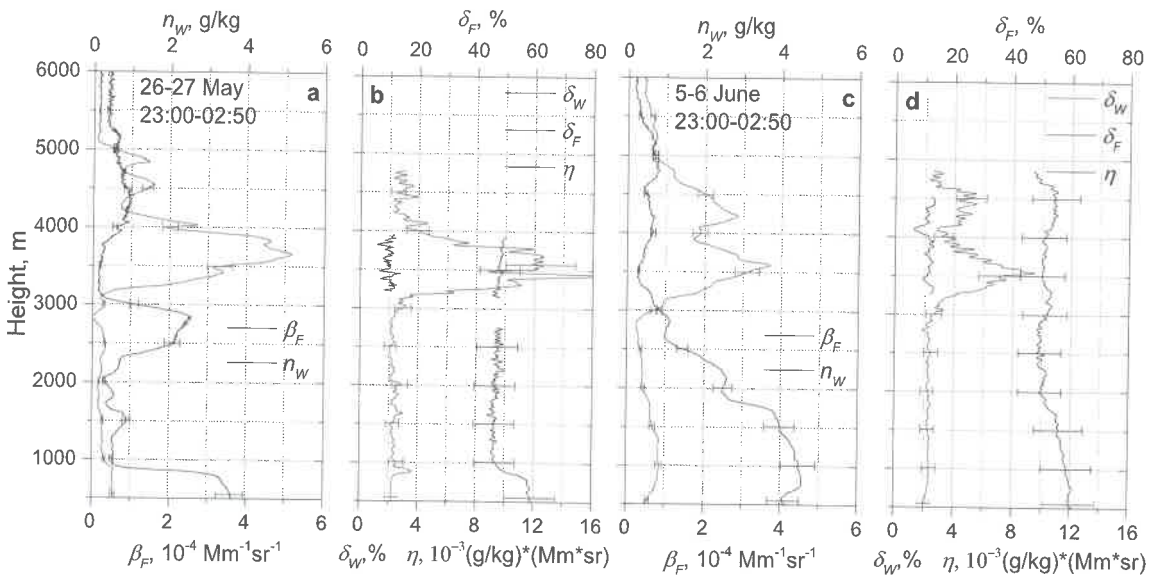

Fig. 13. Fluorescence measurements in Lille on the night 26-27 May and 5-6 June 2023. (a, c) Vertical profiles of the fluorescence backscattering β_F, the water vapor mixing ratio $\tilde{n}_W$, (b, d) the depolarization ratio of water vapor Raman signal $\tilde{\delta}_W$, the fluorescence depolarization ratio δ_F and parameter η, describing contribution of fluorescence to the water vapor channel.

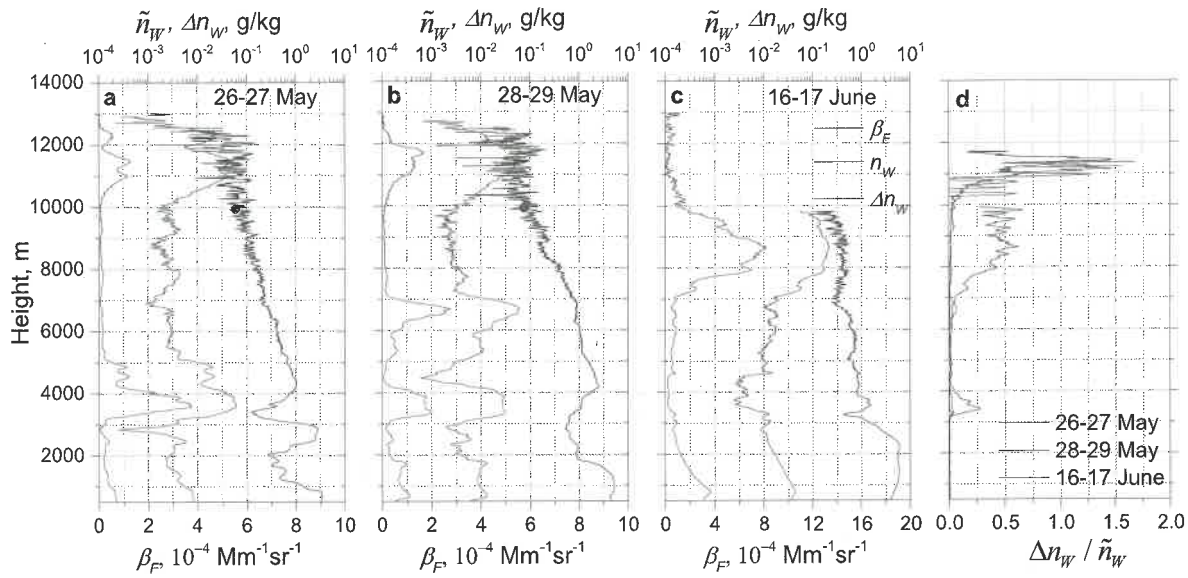

Fig.14. Impact of smoke fluorescence on the water vapor measurements. Vertical profiles of the fluorescence backscattering β_F, water vapor mixing ratio $\tilde{n}_W$ and bias in water vapor channel Δn_W provided by the fluorescence of smoke for episodes on the nights (a) 26-27 May, (b) 28-29 May and (c) 16-17 June 2023 for time interval 21:00-02:30 UTC, (d) Error $\frac{\Delta n_W}{\tilde{n}_W}$ introduced by smoke fluorescence for three episodes.

over .... define city/region.